Racemic Naproxen – a multi-disciplinary structural and thermodynamic comparison with the enantiopure form

Doris E. Braun, Miguel Ardid-Candel, Emiliana D'Oria, Panagiotis G. Karamertzanis, Jean-Baptiste Arlin, Alastair J. Florence, Alan G. Jones and Sarah L. Price

Contents of Supporting Information

A) Computational

1. Conformational Analysis of Naproxen

Conformational energy scans were performed at the PBE/6-31G(d,p) level using GAUSSIAN03.[1] We considered the three main torsion angles in Fig. 1 and performed an optimised scan for the dihedral ϕ_1 and for the combination of the dihedrals ϕ_2 and ϕ_3. The one dimensional scan for ϕ_1 revealed two minima, in which the methoxy group adopts coplanar conformations relative to the naphthalene ring (Figure S1). The global search minimum was found to be 5.1 kJ mol^{-1} more stable than the local minimum. The energy barrier between the two minima is 20.2 kJ mol^{-1}.

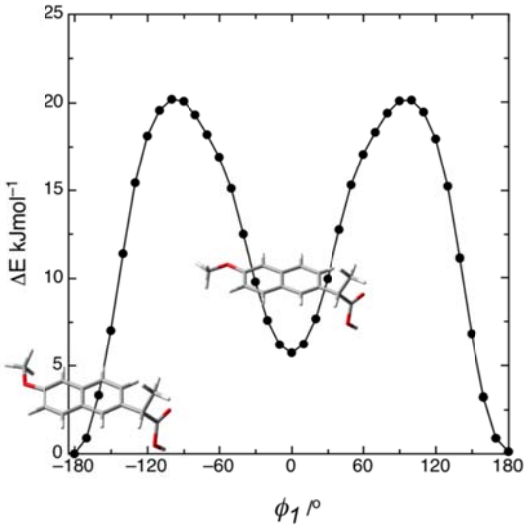

Figure S1. One dimensional potential energy surface scan for naproxen with respect to ϕ_1 ($C_{14}O_1C_7C_8$) at the PBE level of theory with the 6-31G(d,p) basis set. The lowest and second lowest conformations for naproxen are shown in the figure.

A Cambridge Structural Database dihedral angle search (CSD v. 5.32, excluding disordered, ionic and powder structures) was performed on ϕ_1 using the β-methoxynaphthalene moiety. Without any further constraints this resulted in 376 structures (701 fragments) with dihedral angles exclusively being around ± 180° and ± 0°, the two low energy positions found in the one dimensional scan (Figure S2), consistent with Figure S1. Specifying the *ortho* positions of the β-methoxynaphthalene moiety to be protons resulted in 151 structures (202 fragments), which showed an even greater preference for one planar conformation.

Two dimensional scans for the combination of dihedrals ϕ_2 and ϕ_3 (Fig. 1) with ϕ_1 being 179.73° and –0.27°, respectively, each resulted in four minima separated by significant barriers (Figure S3 and Table S1). (One low energy conformation was strictly two close minima with a small barrier). The two conformational energy landscapes (Figure S3 a & b) are very similar, because of the limited

interactions between the methoxy group and the propionic acid group; however the asymmetry from the 2,7 substitution makes these distinct conformations, even if the methoxy group were coplanar. Each of the eight lowest conformers were used as starting points for the rigid body crystal prediction searches, with the geometry optimised at MP2/6-31G(d,p). The conformational minimum closest to that observed in the two experimental structures is the second lowest in energy. Although other conformers are competitive in their intramolecular energy, none of these gave rise to crystal structures within the energy range considered in Figure 4.

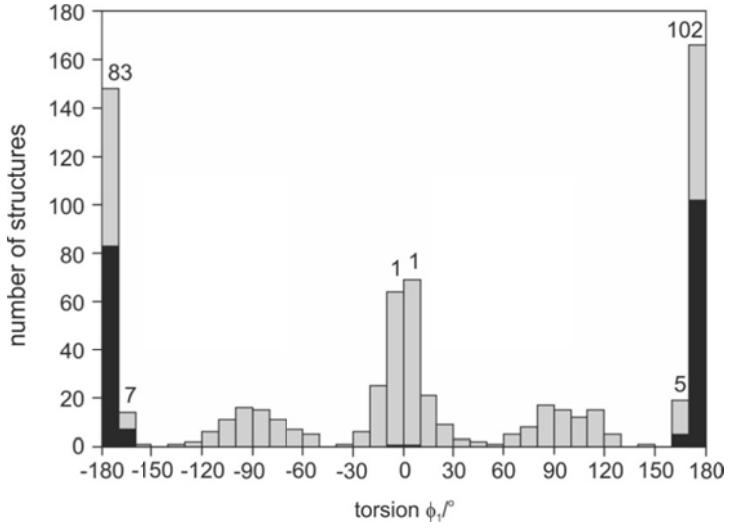

Figure S2. Experimental distribution for the ϕ_1 torsion angle in crystal structures containing β-methoxynaphthalene moiety distinguished by the *ortho* substituent being either a hydrogen atom (black, and numbers) or other group (grey).

Table S1. Relative intramolecular energy differences (ΔE_{intra}) with respect to the global energy minimum of the eight conformers used in the rigid-body crystal structure prediction searches, calculated using different wavefunctions. The conformation closest to that observed in the crystal structures is shaded.

ϕ_1	ϕ_2	ϕ_3	ΔE_{intra}/kJ mol^{-1}					
			MP2/ 6-31G(d,p)	HF/ 6-31G(d,p)	PBE0/ 6-31G(d,p)	MP2/ 6-31G(d,p) PCM(ε=3)[a]	MP2/ 6-31G(d,p) PCM(ε=3)[b]	PBE0/ aug-cc-pVTZ PCM(ε=3)[c]
179.73°	-52.44°	91.49°	0.99	1.46	0.99	0.98	0.82	0.73
179.73°	117.63°	-97.63°	4.91	5.10	5.16	4.45	4.75	4.43
179.73°	-61.12°	-96.08°	6.18	6.90	6.39	5.83	6.00	5.69
179.73°	121.78°	91.49°	0.00	0.00	0.00	0.00	0.00	0.00
-0.27°	-52.44°	91.49°	8.20	9.79	7.26	7.90	7.58	32.59
-0.27°	117.63°	-97.63°	12.00	13.21	11.35	11.23	11.42	36.13
-0.27°	-61.12°	-96.08°	13.64	15.57	12.92	12.95	13.03	37.86
-0.27°	121.78°	91.49°	7.28	8.34	6.38	6.92	6.82	32.00

[a]Single point calculation using the MP2/6-31G(d,p) optimised conformers, [b]single point calculation using the HF/6-31G(d,p) optimised conformers, [c]single point calculation using the PBE0//6-31G(d,p) optimised conformers.

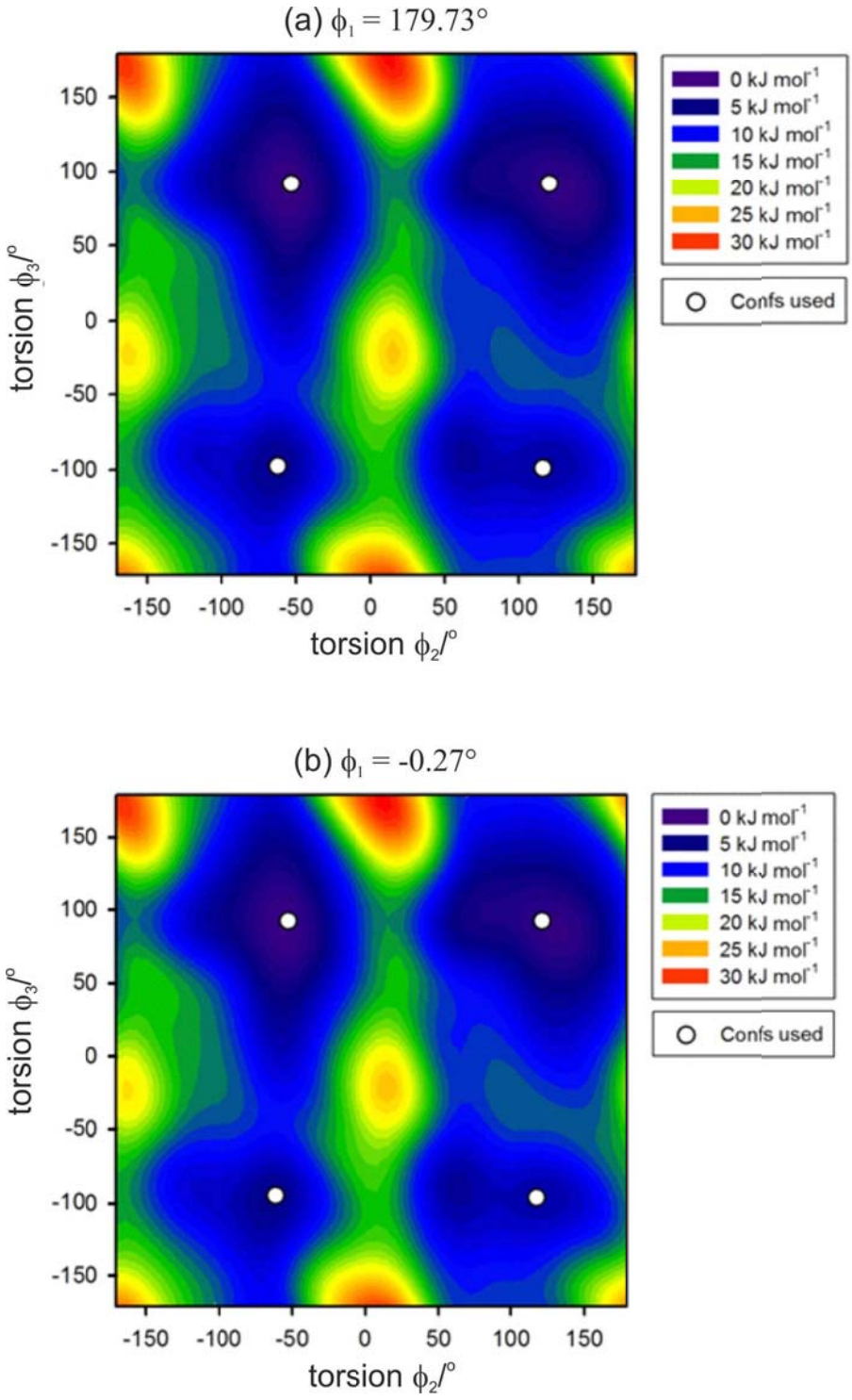

Figure S3. Two dimensional potential energy surface scans for naproxen with respect to ϕ_2 ($C_{12}C_{11}C_2C_1$) and ϕ_3 ($O_2C_{12}C_{11}C_2$) at the PBEPBE level of theory with the 6-31G(d,p) basis set, with the methoxyl torsion (ϕ_1, $C_{14}O_1C_7C_8$) fixed to (a) the optimised value of 179.73° and (b) –0.27°. Conformers used as starting points for the rigid-body searches are marked on the energy landscape in white.

2. Representation of the experimental naproxen structures

The representation of the experimental structures using different modeling techniques is given in Table S2. The model used for the crystal energy landscape is highlighted.

Table S2. The stationary points in the lattice energy (E_{latt} = ΔE_{intra} +U_{inter}) obtained starting from the experimental racemic and enantiomeric naproxen crystal structures, as a function of the wavefunctions used to calculate the conformational energies and multipoles. For ΔE_{intra} method see Table S3.

	Lattice parameters				cell density g cm^{-3}	rmsd$_{15}$[a] (Å)	E_{latt} kJ mol^{-1}
	a/Å	*b*/Å	*c*/Å	*β*/°			
Structure/method U_{inter}	(S)-naproxen (COYRUD11)						
Expt, 25°C	13.375	5.793	7.914	93.91	1.250	-	-
HF/6-31G(d,p)	13.090	5.582	8.291	92.39	1.263	0.38	-137.00
HF/6-31G(d,p), PCM (ε=3)	13.070	5.576	8.294	92.47	1.266	0.39	-143.95
HF/6-31G(d,p), PCM (ε=5)[b]	13.075	5.565	8.310	92.33	1.266	0.39	-146.71
MP2/6-31G(d,p)	13.148	5.608	8.272	92.21	1.255	0.35	-125.11
MP2/6-31G(d,p), PCM (ε=3)	13.080	5.568	8.832	92.31	1.264	0.38	-143.39
MP2/6-31G(d,p), PCM (ε=5)	13.075	5.565	8.310	92.33	1.266	0.39	-146.20
PBE0/6-31G(d,p)	13.137	5.620	8.244	92.23	1.257	0.34	-129.54
PBE0/6-31G(d,p), PCM (ε=3)	13.080	5.568	8.312	92.31	1.264	0.34	-134.42
PBE0/aug-cc-pVTZ (HF)	13.128	5.576	8.301	92.06	1.259	0.39	-131.96
PBE0/aug-cc-pVTZ (PBE0)	13.103	5.585	8.340	91.38	1.253	0.41	-129.77
Structure/method U_{inter}	(RS)-naproxen						
expt, 25°C	25.830	15.494	5.946	90	1.285	-	-
HF/6-31G(d,p)	24.837	17.084	5.495	90	1.312	0.67	-143.74
HF/6-31G(d,p)[c]	24.868	5.456	17.156	90	1.314	0.89	-144.58
HF/6-31G(d,p), PCM (ε=3)	24.852	17.035	5.500	90	1.314	0.66	-150.05
HF/6-31G(d,p), PCM (ε=3)[c]	24.881	5.460	17.108	90	1.316	0.88	-151.12
HF/6-31G(d,p), PCM (ε=5)[b]	24.872	16.932	5.520	90	1.316	0.66	-153.02
HF/6-31G(d,p), PCM (ε=5)[b,c]	24.891	5.470	17.038	90	1.319	0.85	-154.0
MP2/6-31G(d,p)	24.869	17.070	5.518	90	1.306	0.67	-133.69
MP2/6-31G(d,p)[c]	24.888	5.469	17.182	90	1.308	0.89	-134.40
MP2/6-31G(d,p), PCM (ε=3)	24.873	16.950	5.519	90	1.314	0.70	-149.53
MP2/6-31G(d,p), PCM (ε=3)[c]	24.891	5.470	17.056	90	1.317	0.86	-150.50
MP2/6-31G(d,p), PCM (ε=5)	24.872	16.932	5.520	90	1.316	0.66	-152.91
MP2/6-31G(d,p), PCM (ε=5)[c]	24.891	5.470	17.038	90	1.319	0.85	-153.88
PBE0/6-31G(d,p)	24.963	16.907	5.547	90	1.306	0.76	-136.35
PBE0/6-31G(d,p)[c]	24.948	5.481	17.065	90	1.308	0.86	-137.13
PBE0/6-31G(d,p), PCM (ε=3)	24.967	16.858	5.555	90	1.308	0.74	-141.07
PBE0/6-31G(d,p), PCM (ε=3)[c]	24.951	5.487	17.047	90	1.311	0.85	-141.92
PBE0/aug-cc-pVTZ (HF)	24.972	16.792	5.568	90	1.310	0.62	-140.35
PBE0/aug-cc-pVTZ (HF)[c]	24.903	5.466	17.143	90	1.311	0.86	-141.17
PBE0/aug-cc-pVTZ (PBE0)	24.996	16.724	5.619	90	1.302	0.58	-138.17
PBE0/aug-cc-pVTZ (PBE0)[c]	24.943	5.520	17.056	90	1.303	0.85	-139.01

[a]Reproduction of the crystal structures was evaluated by the optimal root-mean square overlay of all non-hydrogen atoms in a 15 molecule coordination cluster (rmsd$_{15}$). [b]HF energy extracted from MP2 calculation. [c]True minimum *Pca*2$_1$ structure (Z'=2), obtained by symmetry reduction of the *Pbca* (Z'=1) transition state.

Table S3. Comparison of calculated lattice energies for the lattice energy minima corresponding to the two experimental NPX crystal structures using different methods for evaluating the conformational energy penalty, ΔE_{intra}, and electrostatic contribution to the intermolecular energy, U_{inter}.

(a) Using the $Pca2_1$ structure (Z'=2) lattice energy minimum for (RS)-NPX

Method U_{inter} atomic multipole	Method ΔE_{intra}	ΔE_{intra}(S)	ΔE_{intra}(RS)	E_{latt}(S)	E_{latt}(RS)	ΔE_{latt} Δ(S)–(RS)
HF/6-31G(d,p)	HF 6-31G(d,p)	2.73	1.61	-137.00	-144.58	-7.58
HF/6-31G(d,p), PCM (ε=3)	Taken from U_{inter}[b]	3.01	1.26	-143.95	-151.12	-7.16
HF/6-31G(d,p), PCM (ε=5)	Taken from U_{inter}[c]	2.44	0.86	-146.71	-154.00	-7.29
MP2/6-31G(d,p)	HF 6-31G(d,p)	2.73	2.04	-125.11	-134.40	-8.29
MP2/6-31G(d,p), PCM (ε=3)[a]	**Taken from U_{inter}[b]**	**3.21**	**1.77**	**-143.39**	**-150.50**	**-7.11**
MP2/6-31G(d,p), PCM (ε=5)	Taken from U_{inter}[c]	2.95	0.98	-146.20	-153.88	-7.68
PBE0/6-31G(d,p)	HF 6-31G(d,p)	1.12	0.81	-129.54	-137.13	-7.59
PBE0/6-31G(d,p), PCM (ε=3)	Taken from U_{inter}[d]	1.78	1.33	-134.42	-141.92	-7.50
PBE0/aug-cc-pVTZ	HF 6-31G(d,p)	1.11	0.81	-131.96	-141.17	-9.21
PBE0/aug-cc-pVTZ	PBE0 6-31G(d,p)	3.30	2.41	-129.77	-139.01	-9.24

(b) Using the corresponding *Pbca* (Z'=1) structure for (RS)-NPX

Method U_{inter} atomic multipole	Method ΔE_{intra}	ΔE_{intra}(S)	ΔE_{intra}(RS)	E_{latt}(S)	E_{latt}(RS)	ΔE_{latt} Δ(S)–(RS)
HF/6-31G(d,p)	HF 6-31G(d,p)	2.73	1.91	-137.00	-143.74	-6.74
HF/6-31G(d,p), PCM (ε=3)	Taken from U_{inter}[b]	3.01	1.70	-143.95	-150.05	-6.10
HF/6-31G(d,p), PCM (ε=5)	Taken from U_{inter}[c]	2.44	1.17	-146.71	-153.02	-6.31
MP2/6-31G(d,p)	HF 6-31G(d,p)	2.73	1.99	-125.11	-133.69	-7.58
MP2/6-31G(d,p), PCM (ε=3)[a]	**Taken from U_{inter}[b]**	**3.21**	**2.08**	**-143.39**	**-149.53**	**-6.14**
MP2/6-31G(d,p), PCM (ε=5)	Taken from U_{inter}[c]	2.95	1.28	-146.20	-152.91	-6.71
PBE0/6-31G(d,p)	HF 6-31G(d,p)	1.12	1.03	-129.54	-136.35	-6.81
PBE0/6-31G(d,p), PCM (ε=3)	Taken from U_{inter}[d]	1.78	1.82	-134.42	-141.07	-6.65
PBE0/aug-cc-pVTZ	HF 6-31G(d,p)	1.11	1.03	-131.96	-140.35	-8.39
PBE0/aug-cc-pVTZ	PBE0 6-31G(d,p)	3.30	3.33	-129.77	-138.17	-8.40

[a]Method as used for generating the crystal energy landscape (Figure 3). [b]HF/6-31G(d,p) (PCM, ε=3) conformational energy penalty taken from single point charge density calculation. [c]HF/6-31G(d,p) (PCM, ε=5) conformational energy penalty taken from single point charge density calculation. [d]PBE0/6-31G(d,p) (PCM, ε=3) conformational energy penalty taken from single point charge density calculation.

3. Computationally generated crystal energy landscape

The hypothetical crystal structures are available in *.res from the authors on request.

Table S4. Hypothetical low-energy crystal structures of naproxen. Known structures are highlighted in grey.

Structure	Space group	Cell parameters						E_{latt}/ kJ mol^{-1}	Density/ g cm^{-3}	H-bonding Motif
		a/Å	b/Å	c/Å	α/°	β/°	γ/°			
Homochiral Structures										
af92	$P2_1$	13.073	5.572	8.306	90	87.60	90	-143.39	1.265	C1,1(4)[ab]
ah12	$P2_1$	13.378	7.473	6.139	90	87.08	90	-139.02	1.248	C1,1(4)[a]
aq49	P212121	14.436	15.281	5.563	90	90	90	-138.73	1.246	C1,1(4)[b]
af41	$P2_1$	5.885	10.996	9.290	90	78.11	90	-131.88	1.300	C1,1(11)
Racemic Structures										
CO_1_SR	$Pca2_1$	24.891	5.470	17.056	90	90	90	-150.50	1.317	R2,2(8)
CO_1	*Pbca*	24.873	16.950	5.519	90	90	90	-149.53	1.314	R2,2(8)
ak57	$P2_1/c$	14.166	5.336	24.349	90	140.94	90	-147.54	1.319	R2,2(8)
fc15	$P2_1/c$	11.270	5.535	20.066	90	71.06	90	-146.61	1.292	R2,2(8)
am85	$P2_1/c$	10.029	5.374	21.875	90	86.13	90	-145.56	1.300	R2,2(8)
fc100	$P2_1/c$	12.106	5.341	18.607	90	84.27	90	-144.34	1.278	R2,2(8)
fb24	$P2_1$	5.363	18.339	12.935	90	69.25	90	-144.31	1.285	R2,2(8)
ak35	$P2_1/c$	12.989	7.203	13.423	90	74.23	90	-143.51	1.266	R2,2(8)
ak63	$P2_1/c$	8.157	5.620	26.845	90	92.29	90	-142.86	1.244	R2,2(8)
ab9	*P*-1	12.683	5.336	9.634	78.50	79.26	70.31	-142.49	1.282	R2,2(8)
fc119	$P2_1/c$	12.004	5.330	19.607	90	105.04	90	-142.10	1.262	R2,2(8)
ca102	*P*-1	11.950	5.386	12.781	101.61	48.98	93.68	-141.19	1.263	R2,2(8)
fa31	$P2_1/m$	5.363	19.061	11.871	90	95.16	90	-140.81	1.266	R2,2(8)
bh18	$Pca2_1$	16.111	13.179	5.699	90	90	90	-140.49	1.264	C1,1(4)
am133	$P2_1/c$	5.331	9.547	24.138	90	95.97	90	-140.34	1.252	R2,2(8)
fc125	$P2_1/c$	13.472	5.748	15.762	90	89.44	90	-140.12	1.253	R2,2(8)
cc56	*Pbca*	5.830	22.775	17.987	90	90	90	-139.32	1.281	C1,1(4)
fa104	$P2_1/c$	11.917	15.126	8.600	90	51.85	90	-139.00	1.255	R2,2(8)
ai123	$P2/c$	21.899	5.192	11.663	90	65.49	90	-138.51	1.268	R2,2(8)
de83	$C2/c$	19.660	5.411	27.578	90	56.03	90	-138.40	1.257	R2,2(8)
am57	$P2_1/c$	7.150	20.727	7.849	90	95.86	90	-137.98	1.322	C1,1(11)
ca69	*P*-1	6.996	12.505	8.034	98.83	64.00	81.24	-137.96	1.264	R2,2(8)
ca79	*P*-1	7.314	10.929	8.170	104.42	107.03	92.84	-137.81	1.276	R2,2(8)
fc83	$P2_1/c$	5.982	7.707	27.004	90	80.98	90	-137.78	1.244	R2,2(8)
ak52	$P2_1/c$	12.215	5.498	22.656	90	128.46	90	-137.73	1.284	R2,2(8)
fc116	$P2_1/c$	5.266	12.039	30.070	90	140.08	90	-137.50	1.250	R2,2(8)
cd 137	*Pbcn*	19.131	5.436	23.408	90	90	90	-137.31	1.257	R2,2(8)
de139	$C2/c$	29.058	5.247	19.352	90	55.92	90	-137.29	1.252	R2,2(8)
ca89	*P*-1	5.465	5.230	22.312	95.06	94.98	74.95	-136.78	1.249	R2,2(8)
ai43	$P2/c$	15.544	5.680	26.786	90	31.85	90	-136.03	1.225	R2,2(8)
CO_70	$Pca2_1$	11.594	40.333	5.201	90	90	90	-135.88	1.258	R2,2(8)
CO_433	*Pbca*	7.575	25.835	12.196	90	90	90	-135.53	1.282	C1,1(4)
ab52	*P*-1	14.806	5.733	9.685	55.83	77.58	65.46	-135.02	1.236	R2,2(8)
ak86	$P2_1/c$	8.458	13.352	11.928	90	65.55	90	-134.95	1.247	R2,2(8)
ca87	*P*-1	5.321	11.291	11.296	73.93	78.45	69.77	-133.90	1.258	C1,1(11)
dc96	$C2/c$	25.863	7.331	24.679	90	31.49	90	-133.40	1.252	R2,2(8)
aw48	*Pba*2	21.148	7.742	7.104	90	90	90	-133.30	1.315	C1,1(11)

Labels for hypothetical structures correspond to internal file names. [a]Contains the stack Fig. 5. [b] contains the catemer arrangement in Fig 5.

B) Experimental

4. Identification of enantiomeric and racemic naproxen

(RS)- and (S)-naproxen exhibit clear differences in their Infrared, Raman and X-ray powder diffraction patterns. Differential scanning calorimetric measurements of the two compounds exhibited very similar melting points (see Table 1). The spectra, diffractograms and DSC curves are given below. All (RS)- and (S)-naproxen crystallization batches matched these spectra.

FT Infrared spectroscopy

Infrared spectra were recorded with a diamond ATR crystal on a Perkin Elmer Spectrum One Fourier Transform spectrophotometer (Perkin Elmer, Norwalk Ct., USA). The spectra were recorded over a range of 4000 to 600 cm^{-1} with a resolution of 2 cm^{-1} (24 scans). Spectra were analyzed with the Opus v 5.5 software.

FT Raman spectroscopy

Fourier Transform Raman (FT-Raman) Spectra were recorded with a Bruker RFS 100 Raman-spectrometer (Bruker Analytische Messtechnik GmbH, D), equipped with a Nd:YAG Laser (1064 nm) as the excitation source and a liquid-nitrogen-cooled, high sensitivity Ge-detector. The spectra (64 scans per spectrum) were recorded in aluminum sample holders with a laser power of 300 mW and a resolution of 2 cm^{-1}.

(a)

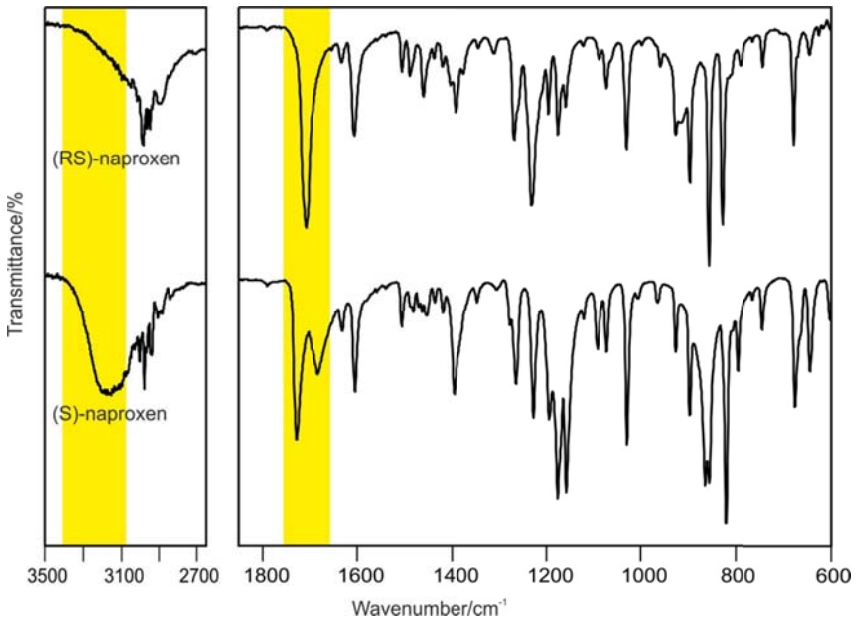

(b)

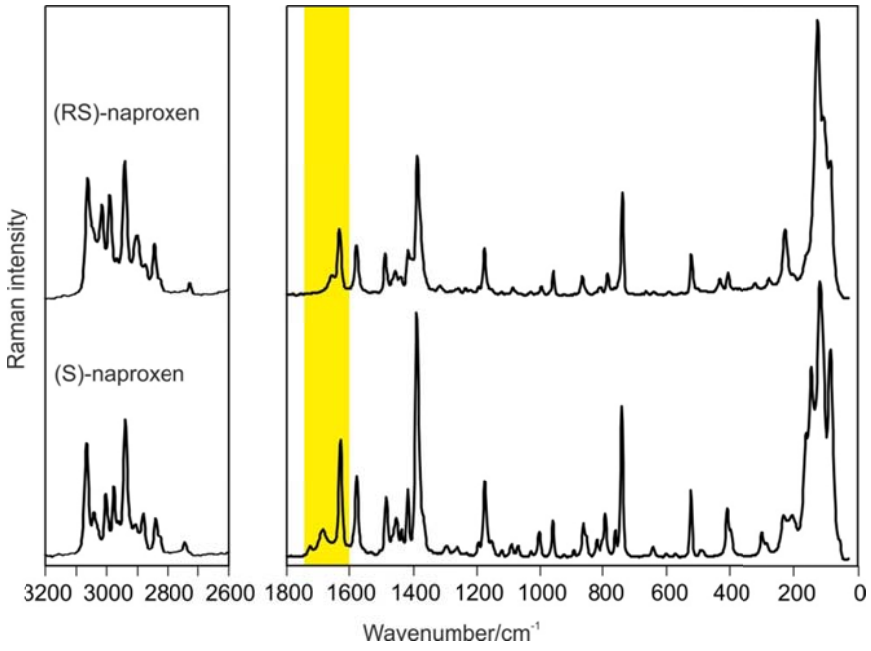

Figure S4. (a) FT-IR spectra of (S)- and (RS)-naproxen. Highlighted are the regions of the C=O and O–H stretching vibrations. (b) FT-Raman spectra of (S)- and (RS)-naproxen. Highlighted are the regions of the C=O stretching vibrations.

Powder X-ray diffractometry

The powder X-ray diffraction patterns used for phase identification were obtained using an X'Pert PRO diffractometer (PANalytical, Almelo, The Netherlands) equipped with a theta/theta coupled goniometer in transmission geometry, programmable XYZ stage with well plate holder, Cu-K$\alpha_{1,2}$ radiation source with a focussing mirror, a 0.5° divergence slit and a 0.02° Soller slit collimator on the incident beam side, a 2 mm antiscattering slit and a 0.02° Soller slit collimator on the diffracted beam side and a solid state PIXcel detector. The patterns were recorded at a tube voltage of 40 kV, tube current of 40 mA, applying a step size of $2\theta = 0.013°$ with 40 s per step in the 2θ range between 2° and 40°.

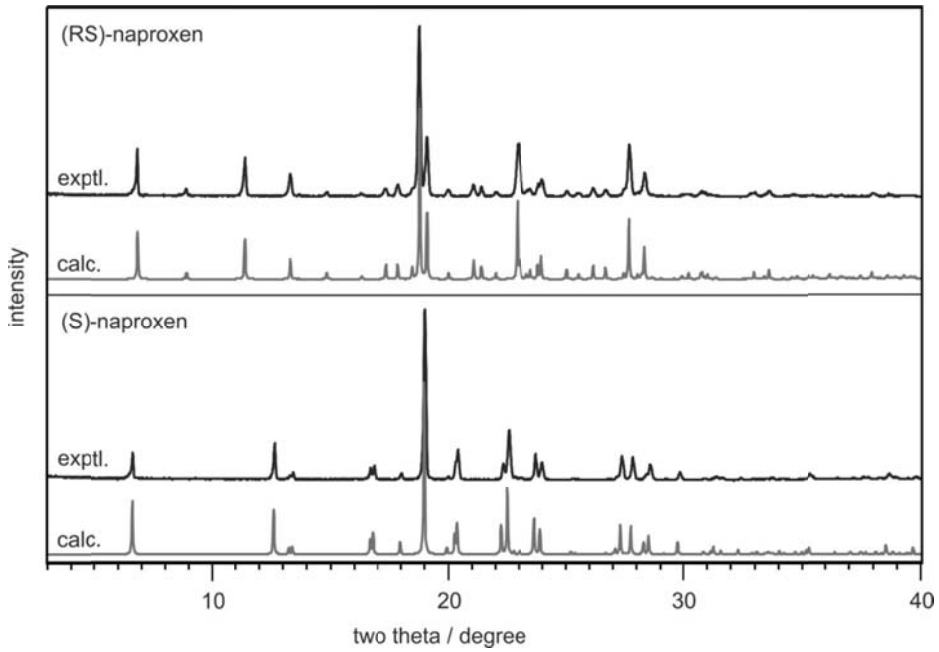

Figure S5. X-ray powder diffraction patterns of (S)- and (RS)-naproxen. The experimental diffractograms are contrasted with the calculated powder patterns (S: single crystal data, COYRUD11, RS: own structure solution).

Differential Scanning Calorimetry (DSC)

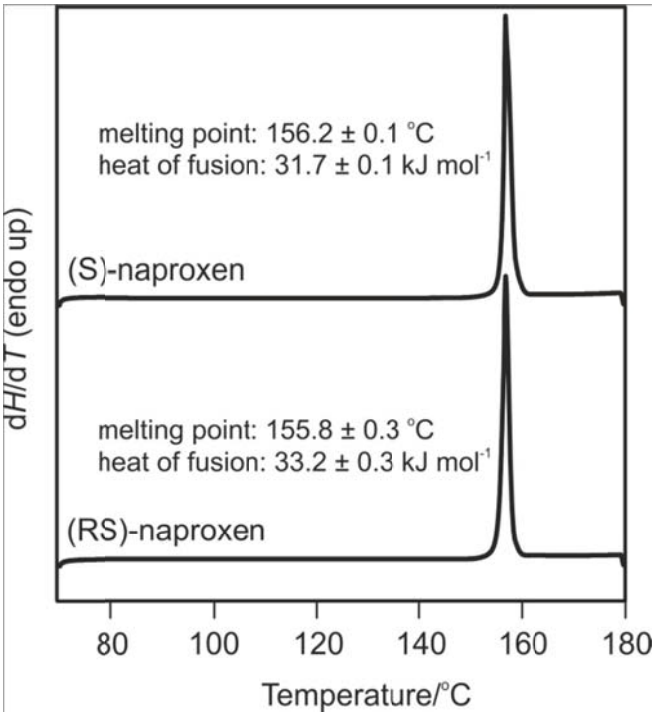

Figure S6. DSC curves of (S)- and (RS)-naproxen (heating rate 10 K min^{-1}).

5. Crystal growth of (RS)-naproxen

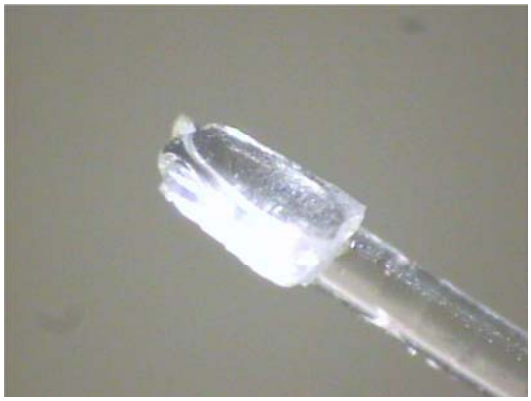

Figure S7. Multilayered (RS)-NPX crystal (size: 0.6 mm *x* 0.3 mm *x* 0.07 mm). This was the largest crystal grown in the attempts to obtain a single crystal over a period of a few months.

6. Structure determination of (RS)-naproxen

Table S5. Variable count time for powder X-ray data collection used for (RS)-NPX structure determination.

2θ range/°	Count time/s per step
3 to 22	2
22 to 40	5
40 to 55	12
55 to 70	24

7. Solid state NMR of (RS)-naproxen

Solid-state NMR spectroscopy of (RS)-naproxen was performed at the University of Durham (EPSRC National Solid-state NMR Research Service). Carbon-13 cross-polarization magic-angle spinning (CPMAS) spectra at ambient probe temperature were obtained at 100.56 MHz, using a Varian VNMRS spectrometer based on a 9.4 T Oxford Instruments superconducting magnet. The probe accepts 6.0 mm (outside diameter) zirconia "pencil" rotors, which were fitted with Teflon end-caps. Proton decoupling with the TPPM protocol at power equivalents to frequencies of 53.2 kHz was employed during acquisition of $_{13}$C. The MAS rate was 6.8 kHz. Contact times for the CP experiments were 3ms.

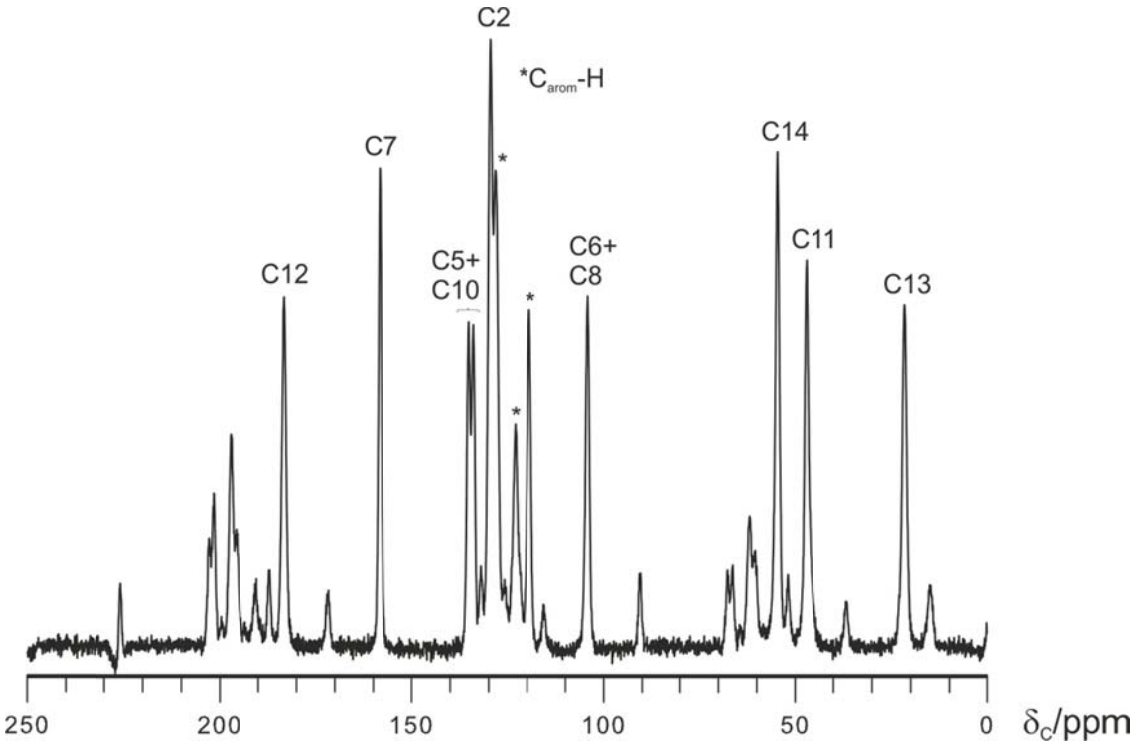

Figure S8. Carbon-13 CPMAS spectra of (RS)-naproxen.

8. Ideal solubilities

Table S6. Ideal solubilities at several temperatures of (RS)- and (S)-naproxen calculated from melting point data.

Temperature/°C	(RS)-NPX/ mole fraction	(S)-NPX/ mole fraction
10	7.920 x 10^{-3}	9.823 x 10^{-3}
15	9.711 x 10^{-3}	11.931 x 10^{-3}
20	11.865 x 10^{-3}	14.442 x 10^{-3}
25	14.449 x 10^{-3}	17.426 x 10^{-3}
30	17.357 x 10^{-3}	20.960 x 10^{-3}
35	21.218 x 10^{-3}	25.135 x 10^{-3}
40	25.593 x 10^{-3}	30.053 x 10^{-3}

9. Author Contributions

Author	Contribution to manuscript
Doris E. Braun	• Computational modelling of the experimental structures • PCM calculations on crystal energy landscape • Thermal measurements (Hot-stage microscopy and Differential Scanning Calorimetry) • Solubility Experiments (assistance) • Analysis of computational and experimental data, discussion of results • Drafting of manuscript
Miguel Ardid-Candel	• Crystallisation experiments • Preparation of samples for thermal measurements • Thermal measurements (Differential Scanning Calorimetry) • Solubility Experiments
Emiliana D'Oria	• Conformational analysis • Crystal structure predictions • Analysis of computational data and discussion of results • Early drafting of manuscript
Panagiotis G. Karamertzanis	• Project idea • Discussion of results
Jean-Baptiste Arlin	• Structure determination of (RS)-naproxen
Alastair J. Florence	• Structure determination of (RS)-naproxen • Discussion of (RS)-naproxen structure
Alan G. Jones	• Project Leader
Sarah L. Price	• Analysis of computational data, discussion of results • Polishing of manuscript